

First Evidence of N_f -Dependence in the QCD Interquark Potential.

SESAM-Collaboration:

U. Glässner^b, S. Güsken^b, H. Hoerber^a, Th. Lippert^a,
G. Ritzenhöfer^a, K. Schilling^{a,b}, G. Siegert^a, A. Spitz^b and A. Wachter^a.

^aHLRZ c/o KFA Jülich, D-52425 Jülich, and DESY, D-22603 Hamburg, Germany,

^bPhysics Department, University of Wuppertal, D-42097 Wuppertal, Germany.

August 1, 2018

Abstract

We present a lattice calculation of the interquark potential between static quarks in a “full” QCD simulation with 2 flavours of dynamical Wilson-quarks at three intermediate sea-quark masses. We work at $\beta = 5.6$ on lattice size of $16^3 \times 32$ with 100 configurations per sea-quark mass. We compare the full QCD potential with its quenched counterpart at equal lattice spacing, $a^{-1} \simeq 2.0$ GeV, which is at the onset of the quenched scaling regime. We find that the full QCD potential lies consistently below that of quenched QCD. We see no evidence for string-breaking effects on these lattice volumes, $V \simeq (1.5 \text{ fm})^3$.

1 Introduction

Ever since the seminal paper of Creutz[1] on the confining character of the static quark-antiquark interaction in the weak coupling regime of quenched QCD, refined lattice methods have been devised and targeted towards an improved determination of the interquark potential. By now, quenched studies on large lattices ($\geq 32^4$) have reached a statistical accuracy in the percent region at small and medium interquark separations, R , for bare lattice couplings in the scaling regime $6.0 \leq \beta \leq 6.8$ [2, 3, 4]. This corresponds to lattice resolutions in the range $1.94 \leq a^{-1} \leq 6$ GeV, which is fine enough to observe running coupling effects[5]¹.

As *full* QCD lattice simulations with Wilson fermions are presently still in their infancy it is rather obvious to ask the question whether the form of the static potential can provide a decent signal for fermion loop effects in the real QCD vacuum state. The shape of the static potential is expected to grow more convex as effects from dynamic fermions turn gradually stronger with decreasing quark mass; however, this can only be observed provided we can access a large enough window of observation in R at sufficiently small quark masses. We can estimate the effect of dynamical fermions on the Coulomb-term of the potential from the lowest-order coupling constant :

$$\alpha(R) \simeq -\frac{1}{8\pi} \frac{1}{b_0 \log R\Lambda_V} , \quad (1)$$

where the N_f -dependence is in b_0 (N_f denotes the number of flavours):

$$b_0 = \frac{33 - 2N_f}{48\pi^2} . \quad (2)$$

¹At present, such level of precision is extremely hard to realize in lattice evaluations of hadronic attributes proper, even in quenched QCD, since this requires very high statistics[6, 7, 8, 9].

Naively, from b_0 only, we would expect to observe an effect on the order of +14 % when switching from $N_f = 0$ to $N_f = 2$. Obviously, to be sensitive to unquenching, one requires data with an overall error (statistical *and* systematic) below the 5 % level. Such a precision was clearly not reached by previous lattice studies with dynamical Wilson fermions [10, 11] in the scaling regime, which we expect to start at $\beta \gtrsim 5.6$.²

In this paper, as part of our ongoing 100 Teraflopshrs simulation of 2-flavour Wilson-fermion QCD, which was described in Ref.[13], we will present a first high statistics study of the interquark potential. We work at a bare lattice coupling of $\beta = 5.6$ on a lattice volume of $16^3 \times 32$ and simulate at three sea-quark masses which correspond to the hopping parameter values $\kappa_{\text{sea}} = 0.156, 0.157$ and 0.1575 . With these parameters the lattice resolution is expected to be around $a^{-1} \simeq 2$ GeV [10, 13, 14].

Field configurations are produced on Quadrics QH2 machines using the Hybrid Monte Carlo Algorithm; for details we refer the reader to a forthcoming publication[15]. In this analysis, we exploit 2500 trajectories per sea-quark mass³, which corresponds to three times 100 independent configurations (see section 2).

2 The Static Potential

Autocorrelation The statistical quality of a sample of configurations generated as an HMC timeseries is largely determined by the integrated autocorrelation time τ_{int} . We have obtained clean signals both for exponential and integrated autocorrelation times of the plaquette using the complete sets of trajectories. In table 1 we list the values for the integrated autocorrelation time τ_{int} . Since the plaquettes are con-

κ_{sea}	0.156	0.1570	0.1575
τ_{int}	4.8(7)	5.1(8)	14.8(8)

Table 1: Exponential and integrated autocorrelation times of the plaquette.

sidered to represent the worst case with respect to autocorrelations we choose to perform measurements on configurations separated by 25 trajectories (a detailed discussion of autocorrelation issues follows in a forthcoming publication)⁴.

Analysis Method The static (spin independent) potential $V(R)$ is computed in a standard fashion from the path-ordered products of link variables around space-time rectangles. In order to enhance the ground-state signal, we use a local gauge-invariant APE-type [16] smearing procedure on the spatial links. The smearing parameter α is set to $\alpha = 2$. We have optimised the number N of smearing iterations and find $N = 20$ or $N = 25$ to yield overlaps ≥ 80 % for all \hat{R} with very little dependence on \hat{R} (lattice quantities are hatted to avoid confusion).

Similarly to the quenched case [4], off-axis measurements are included for improved spatial resolution; this also allows an investigation of rotational invariance restoration. We perform measurements at 36 different values of \hat{R} comprising 8 on-axis and 24 off-axis constellations.

The potential is defined through local masses at time \hat{T} : $\hat{V}^{\hat{T}}(\hat{R}) = \log \frac{\mathcal{W}(\hat{R}, \hat{T})}{\mathcal{W}(\hat{R}, \hat{T}+1)}$. We search for

²In this situation, one is tempted to assess the impact of dynamical fermions by matching, at given values of β and κ_{sea} , the Wilson loops $W(R \times T)$ onto their respective quenched analogues, by suitable β -shifts, $\Delta\beta(R \times T, \beta, \kappa_{\text{sea}})$. Using this technique ref. [10] indeed found an increasing $\Delta\beta$ with R . However, as this procedure can only be related to physical quantities in the large T limit one would prefer to investigate the QCD potential directly [12].

³This is approximately half of our scheduled sample.

⁴Note that due to a variable step size ($N_{\text{md}}^{\text{mean}} = 100$ and $N_{\text{md}}^{\text{var}} = 20$) these configurations are not equidistant in molecular dynamics time.

plateaus defined by

$$\frac{\hat{V}^{\hat{T}-1}(\hat{R})}{\hat{V}^{\hat{T}}(\hat{R})} \simeq 1 . \quad (3)$$

Good plateaus are found for $\hat{T} \geq 3$. We have checked that local masses, $\hat{V}^{\hat{T}}(\hat{R})$, and semi-local masses, from constant fits of $\hat{V}^{\hat{T}}$ on three time-slices $\hat{T} = 3, 4, 5$, yield the same values for the potential. Furthermore, the central values of the fit-parameters (as given below in tables 2 and 3) remain virtually unaffected: however, using semi-local masses one may reduce the errors by approximately 15 % (albeit at the cost of a slightly increased χ^2 per degree of freedom).

Lattice artefacts in the potential due to the difference of the one-gluon exchange on the lattice and in the continuum are corrected for by subtracting a term proportional to

$$\delta\hat{V}(\hat{R}) = \left(\left[\frac{1}{\hat{R}} \right] - \frac{1}{\hat{R}} \right) , \quad (4)$$

where $\left[\frac{1}{\hat{R}} \right]$ denotes the lattice one gluon exchange extrapolated to infinite volume [4, 17, 18]:

$$\left[\frac{1}{\hat{R}} \right] = 4\pi \lim_{V \rightarrow \infty} G(\hat{R}; V) \quad \text{with} \quad G(\hat{R}; V) = \frac{1}{V} \sum_{\hat{k}_i} \frac{\prod_i \cos(\hat{k}_i \hat{R}_i)}{4 \sum_i \sin^2(\hat{k}_i/2)} , \quad (5)$$

where $\hat{k}_i = \frac{2\pi}{L} m_i$, $m_i = -L/2 + 1, \dots, L/2$, $V = L^3$.

In order to fix the size of the correction term $g\delta\hat{V}$ we interpolate our data using the following four-parameter ansatz (the detailed form of the fit is of no interest here, we only wish to show that a smooth interpolation can be obtained):

$$\hat{V}(\hat{R}) = \hat{V}_0 + \hat{k}\hat{R} - \frac{c}{\hat{R}} + g\delta\hat{V}(\hat{R}) . \quad (6)$$

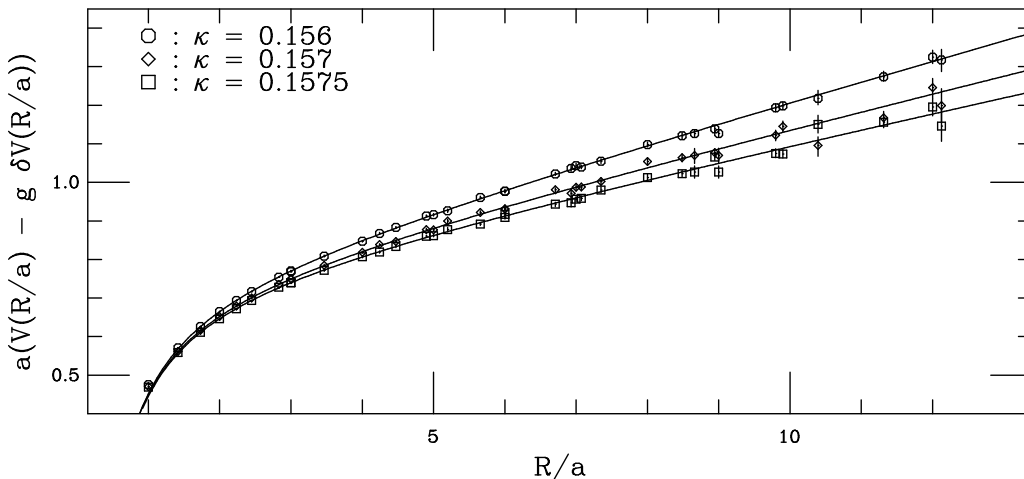


Figure 1: $\left(\hat{V}(\hat{R}) - g\delta\hat{V}(\hat{R}) \right)$ as a function of the lattice separation \hat{R} .

Results The data and fits are shown in figure 1 where we plot $\left(\hat{V}(\hat{R}) - g\delta\hat{V}(\hat{R}) \right)$ as a function of the lattice separation \hat{R} . Throughout the analysis we exclude the two smallest \hat{R} values from the fit⁵. The

⁵These points are, however, included in figure 1.

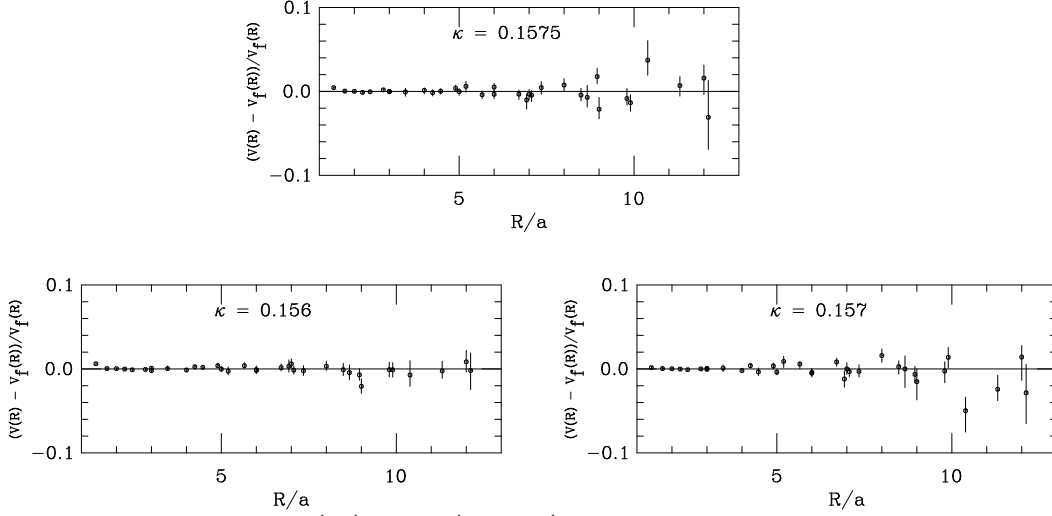


Figure 2: Relative deviations $(\hat{V}(\hat{R}) - V_f(\hat{R}))/V_f(\hat{R})$ of the potential values from the fit curves $V_f(\hat{R})$, eq. 6.

resulting parameters are given in table 2; errors are obtained from a bootstrap sample of size 250 and correspond to 68 % confidence level. We find all χ^2 per degree of freedom to be around 1.

κ_{sea}	\hat{V}_0	\hat{k}	e	g	$\chi^2 / \text{d.o.f}$
0.156	0.724^{+7}_{-6}	0.0514^{+13}_{-12}	0.324^{+9}_{-8}	0.36^{+1}_{-2}	18/30
0.157	0.721^{+8}_{-6}	0.0445^{+10}_{-11}	0.316^{+11}_{-8}	0.35^{+2}_{-2}	31/30
0.1575	0.728^{+7}_{-7}	0.0396^{+13}_{-11}	0.323^{+10}_{-10}	0.37^{+2}_{-2}	25/30
quenched					
6.0	0.6591^{+43}_{-43}	0.04771^{+81}_{-81}	0.2917^{+59}_{-59}	0.2916^{+74}_{-74}	10/29
6.2	0.6336^{+24}_{-24}	0.02574^{+34}_{-34}	0.2865^{+46}_{-46}	0.265^{+11}_{-11}	43/63

Table 2: Fit results from the ansatz eq. 6. For a discussion of the quenched data see section 4.

A more detailed view of the quality of the data and the parametrisation can be obtained by looking at the relative deviations of the data points from the interpolating curves as shown in figure 2. We find the deviations to be smaller than $\pm 2\%$ with minor exceptions at very large \hat{R} . We conclude that adding a term proportional to $\delta\hat{V}(\hat{R})$ is sufficient to remove lattice artefacts at small R and that our interquark potentials show no sign of non-linear behaviour towards large R , as predicted from string breaking.

3 Scaling the data

In the case of full QCD it is appropriate to find the lattice scale from a quantity defined at an intermediate distance rather than using the asymptotic quantity “string-tension”. Therefore, following ref. [19], we extract the lattice spacing a_F by matching the force from our lattice potential to the force obtained from potential models as applied to quarkonium spectroscopy. This amounts to finding the numerical solution, in terms of \hat{R}_0 , of the equation

$$\hat{R}_0^2 \frac{d\hat{V}}{d\hat{R}} \Big|_{\hat{R}_0} = 1.65, \quad (7)$$

which, in phenomenological models, is given by the reference length

$$R_0 = a_F \hat{R}_0 = 0.5 \text{ fm} . \quad (8)$$

Since this procedure involves the use of a numerical derivative it is clearly more delicate than setting the scale by the string-tension and hence requires precise data.

The force values are calculated from the finite differences

$$\hat{F}(\bar{R}) = \frac{\hat{V}_c(\hat{R}_2) - \hat{V}_c(\hat{R}_1)}{(\hat{R}_1 - \hat{R}_2)} , \quad (9)$$

where $\hat{V}_c(\hat{R})$ are the corrected data which we view as our lattice estimates of the continuum QCD potential :

$$\hat{V}_c(\hat{R}) = \hat{V}(\hat{R}) - g\delta\hat{V}(\hat{R}) . \quad (10)$$

All possible pairs of potential data with distances $1.4 \geq (\hat{R}_1 - \hat{R}_2) \geq 1$ are used to calculate an improved \bar{R} in eq. 9 by demanding that

$$-\frac{\partial V_{\text{theo}}(\bar{R})}{\partial \bar{R}} = F(\bar{R}) , \quad (11)$$

where

$$V_{\text{theo}}(R) = V_0 + kR - \frac{e}{R} . \quad (12)$$

Eq. 11 is then solved for \bar{R} using the fit parameters of table 2.

The resulting values \hat{R}_0 and lattice spacings a_F are given in table 3. We find very little difference between the values of \hat{R}_0 obtained from this numerical difference procedure and those obtained analytically, with the fit parameters of eq. 6 :

$$\hat{R}_0 = \sqrt{\frac{1.65 - e}{\hat{k}}} . \quad (13)$$

This is taken as further evidence of the smoothness of our data and as an indication for the stability of the method. Note that the statistical errors are as low as 3 %.

κ_{sea}	\hat{R}_0	$a_F^{-1}[\text{GeV}]$	$a_V^{-1}[\text{GeV}]$
0.156	5.13_{-8}^{+7}	2.02_{-3}^{+3}	1.94_{-2}^{+2}
0.157	5.55_{-17}^{+17}	2.19_{-7}^{+7}	2.09_{-2}^{+3}
0.1575	5.83_{-12}^{+11}	2.30_{-5}^{+4}	2.21_{-3}^{+3}
quenched			
6.0	5.35_{-3}^{+2}	2.11_{-1}^{+1}	2.02_{-1}^{+1}
6.2	7.27_{-3}^{+3}	2.86_{-1}^{+1}	2.74_{-1}^{+1}

Table 3: Lattice spacings obtained from the force at $R_0 = 0.5$ fm and from the string tension $\hat{k} = a^2 \times 0.1936 \text{ GeV}^2$ (see table 2 for \hat{k}). Errors are statistical only. The quenched data are discussed in section 4.

As we see no deviation of the potential from a linear behaviour for large R we can also attempt to extract the lattice spacing from the force at larger distances, i.e. at around 1 fm, where our data are dominated by the linear term in eq. 6. In practical terms, we then interpret the values of \hat{k} from table 2 as string-tension values from which we derive the lattice spacings $a_V = \sqrt{\hat{k}/\sigma}$, where we take, somewhat arbitrarily, $\sqrt{\sigma} = 0.44 \text{ GeV}$ (see table 3). Note that the sizes of the statistical errors are beginning to

be competitive to those of previous quenched calculations (without link-integration) [4, 20]. Moreover, we observe that the ratio a_F/a_V remains unchanged for all three sea-quark masses indicating that a slightly different choice of $\sqrt{\sigma}$, which we find to be 458 ± 12 MeV for $\kappa = 0.1575$, renders consistent lattice spacings from both schemes.

We comment that our hadron spectrum analysis yields lattice spacings consistent with those of table 3, when using the mass of the ρ to set the scale [14].

In figure 3 we show our results in scaled form. We find that the data collapse to a universal potential over the complete range of our measurements, $R \in [0.1, 1.5]$ fm. An analysis similar to that of figure 2

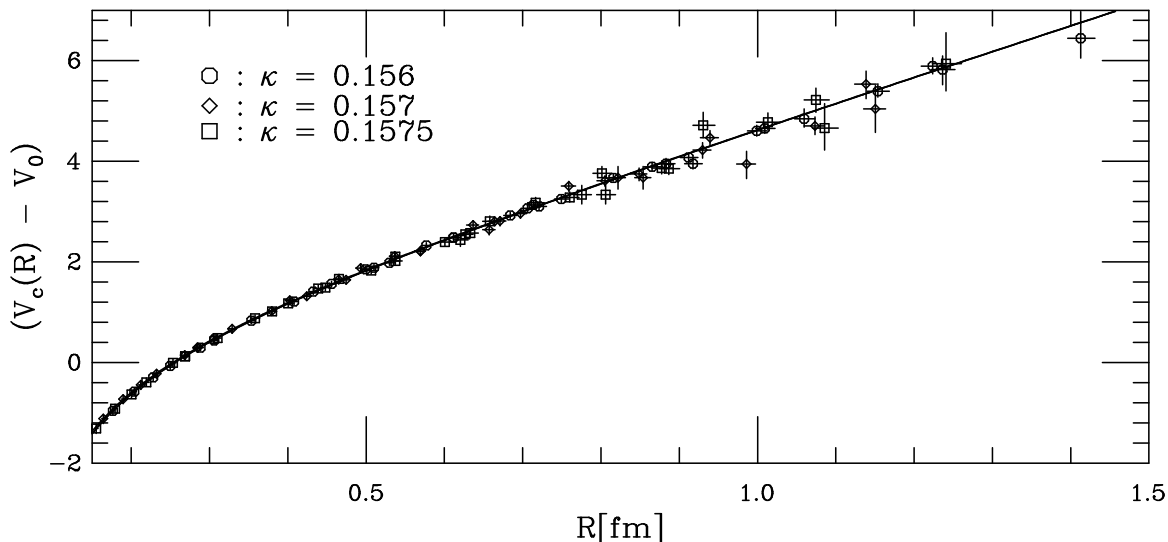


Figure 3: Scaled potential (using a_V) in physical units.

shows that nearly all points lie within ± 2 % of the universal curve.

4 Discussion : effects of dynamical fermions ?

At first sight, it might seem disappointing to find that our scaled data collapse to a universal function; clearly, this shows that the variation of κ_{sea} from 0.156 to 0.1575 is too small to resolve mass-dependence in the static potential. However, we can do more/better by comparing our data to the extreme case, the case of infinitely heavy sea quarks, that is, the quenched approximation.

Table 3 shows that the lattice spacings in the present calculation correspond to quenched couplings slightly above $\beta = 6.0$. We therefore performed two high statistics runs in pure gauge theory including link-integration at $\beta = 6.0$ (lattice size 16^4 , 570 configurations) and $\beta = 6.2$ (lattice size 32^4 , 100 configurations) [21], the $\beta = 6.2$ simulation being done to investigate scaling. In order to achieve comparable systematic errors the evaluation of the quenched potential data and their analysis follow the same procedure as described in section 2 and we perform four-parameter fits at both β -values using a common lower cut $R > 0.196$ fm, designed to give good $\chi^2/d.o.f.$ for all fits⁶.

⁶We have checked however, that varying the fit range to include more values of $V(R)$ at smaller R leaves our conclusions largely unaffected. The fit parameters for the full QCD case are, in fact, completely stable.

Results are shown in tables 2 and 3. We find the quenched data, whose lattice spacings vary by about 40 %, to fall upon a universal curve with deviations smaller than 1 %, corroborating the earlier results of ref [4]. Furthermore, since the lattice spacings at $\beta_{N_f=0} = 6.0$ roughly correspond to those of $\beta_{N_f=2} = 5.6$ (see table 3) we are indeed at the onset of the scaling regime for our full QCD simulation.

The comparison of quenched and unquenched QCD is shown in figure 4 where we plot the data in the small R -region, $R < 0.4$ fm. We find the full QCD data to lie significantly below that of quenched QCD ! In this scaling representation the data are solely sensitive to the strength of the Coulombic term e . In order to quantify the effect of dynamical fermions we can therefore directly extract the information from the e -values as quoted in table 2. As for both cases, full and quenched QCD, we observe good scaling, we can represent each data-set by its appropriate average value, $e_{N_f=2} = 0.3210(100)$ and $e_{N_f=0} = 0.2890(55)$. From these numbers, we find unquenching to induce a decrease of 11 % in the coulombic part of the static potential.

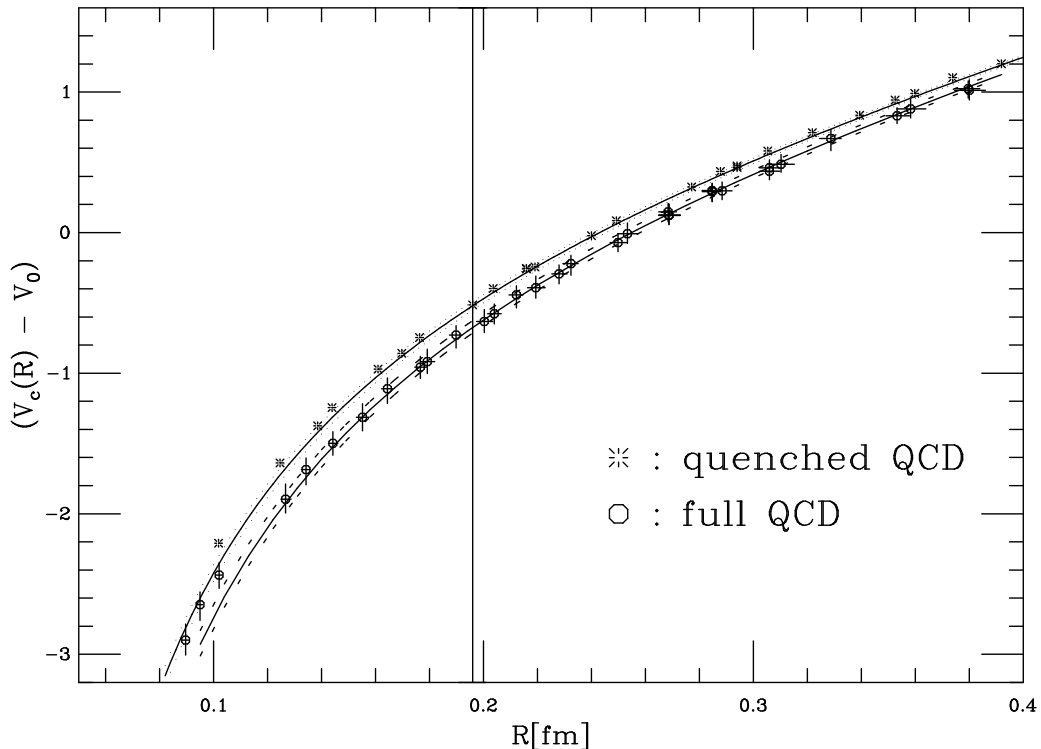


Figure 4: Comparison of scaled potentials from quenched and full QCD (combined data for quenched ($\beta = 6.2$ and $\beta = 6.0$) and full (three sea-quark values) QCD). The plot shows both fits with their one-sigma errorbands where only points right of the vertical line were used for fits, $R \in [0.196, \infty]$ fm.

5 Summary and conclusions

We have presented a calculation of the static potential which is precise enough to unravel, for the first time, the effects of unquenching at intermediate distances. We find the full QCD coupling constant to lie consistently above that of quenched QCD. However, the data are not sensitive enough to see variation of the potential with the sea-quark mass. Our method is based on a consistent modelling of the $N_f = 2$ and $N_f = 0$ potentials. The full QCD lattice spacings are in the range $a^{-1} \simeq 2$ GeV which, in the quenched case, is at the onset of the scaling regime, $\beta_{N_f=0} \simeq 6.0$. Our result is in accord with the N_f -dependence of α as extracted from the perturbative expansion of the plaquette (see for example [23]).

The lattice volume of $(1.5 \text{ fm})^3$ was not large enough to observe string breaking. Note that using quenched data, one can obtain an upper bound for the distance at which string breaking should be observable to be at 1.7 fm [24].

We are currently performing a simulation with the same lattice-resolution but 50 % extended lattice size, in order to assess finite-size effects and to work at lighter quark masses [22].

We are encouraged by these results in our systematic search for Sea quark Effects on Spectrum And Matrix elements.

Acknowledgements We are grateful to DESY and to the DFG for granting substantial amounts of computer time on their QH2 Quadrics systems (at DESY/IfH in Zeuthen and the University of Bielefeld) which was instrumental to creating the QCD vacuum field configurations, and to the IAA of the Bergische Universität Wuppertal, where we could use the CM5 to extract the QCD potential data. Our project and the CM5 in Wuppertal have both been supported by Deutsche Forschungsgemeinschaft through grants Schi 257/1-4 and 257-3-2(3). The quenched computations have partly been done on the 64 node CM5 system of the GMD. TL and KS appreciate support by EU contract CHRX-CT92-0051 which enabled us to build up a cooperation with our colleagues from the INFN Pisa and Roma whom we admire for building, with APE, a very functional hardware for doing computational physics.

References

- [1] M. Creutz., Phys. Rev. **D21** (1980), 2308.
- [2] S. Booth et al.(UKQCD), Phys. Lett. **B294** (1992), 385.
G.S. Bali and K. Schilling, Phys. Rev. **D46** (1992), 2636.
- [3] G.S. Bali, K. Schilling and A. Wachter, HLRZ-95-30, hep-lat/9506017.
- [4] G.S. Bali and K. Schilling, Phys. Rev. **D47** (1993), 661.
- [5] G.S. Bali and K. Schilling, Nucl. Phys. Proc. Suppl. 30 (1993), 453-456.
- [6] F. Butler et al., Nucl. Phys. **B421** (1994), 217 and Nucl. Phys. **B430** (1994), 179.
- [7] S. Aoki et al.(JLQCD), to be published in Nucl. Phys. **B** (Proc. Supp. of Lat. 95, Melbourne); UTHEP-323, hep-lat/9510013.
- [8] T. Bhattacharya et al., preprint LA-UR-95-2354, hep-lat/9512021.
- [9] M. Goeckeler et al., DESY-96-003, hep-lat/9601007.
- [10] R. Gupta et al., Phys. Rev. **D44** (1991), 3272.
- [11] K. M. Bitar et al.(HEMCGC), Phys. Rev. **D49** (1994), 3546.
- [12] K. D. Born et al.(MTC), Phys. Lett. **B329** (1994), 325.

- [13] SESAM–Collaboration, QCD with dynamical Wilson fermions—first results from SESAM, to be published in Nucl. Phys. **B** (Proc. Supp. of Lat. 95, Melbourne); HLRZ-95-57, hep-lat/9510001.
- [14] SESAM–Collaboration, Spectrum and Decay Constants in Full QCD, in preparation.
- [15] SESAM–Collaboration, Toolkit for HMC Practitioners, HLRZ preprint 8/96, in preparation.
- [16] M. Albanese et al., Phys. Lett. **B192** (1987), 163.
- [17] C. Michael, Phys. Lett. **B283** (1992), 103.
- [18] C. B. Lang and C. Rebbi, Phys. Lett. **B115** (1982), 137.
- [19] R. Sommer, Nucl. Phys. **B411** (1994), 839.
- [20] H. Wittig (UKQCD), Nucl. Phys. **B42** (Proc. Supp.) (1995).
- [21] G.S. Bali, K. Schilling and A. Wachter, in preparation.
- [22] T χ L - Collaboration, L. Conti, L. Giusti, U. Glässner, S. Güsken, H. Hoerber, Th. Lippert, G. Martinelli, F. Rapuano, G. Ritzenhöfer, K. Schilling, G. Siegert and A. Spitz; in preparation.
- [23] S. Aoki et al., Phys. Rev. Lett. **74** (1995), 22.
- [24] C. Alexandrou et al., Nucl. Phys. **B414** (1994), 815.